Clinical Radiology 74 (2019) 456–466

Contents lists available at ScienceDirect

Clinical Radiology

journal homepage: www.clinicalradiologyonline.net

Spectral CT and its specific values in the staging of patients with non-small cell lung cancer: technical possibilities and clinical impact

U. Fehrenbach [a,1], J. Kahn [a,1], G. Böning [a], F. Feldhaus [a], K. Merz [a], N. Frost [b], M.H. Maurer [c], D. Renz [d], B. Hamm [a], F. Streitparth [a,e,*]

[a] *Department of Radiology, Charité University Medicine Berlin, Campus Virchow Klinikum, Berlin, Germany*
[b] *Department of Internal Medicine — Pulmonology, Charité University Medicine Berlin, Campus Virchow Klinikum, Berlin, Germany*
[c] *Department of Radiology, University Hospital/Inselspital Bern, Bern, Switzerland*
[d] *Department of Radiology, University Hospital Jena, Jena, Germany*
[e] *Department of Radiology, University Hospital Munich, Ludwig-Maximilians University (LMU), Munich, Germany*

ARTICLE INFORMATION

Article history:
Received 20 October 2018
Accepted 12 February 2019

AIM: To investigate how spectral computed tomography (SCT) values impact the staging of non-small cell lung cancer (NSCLC) patients.

MATERIALS AND METHODS: One hundred and thirteen patients with confirmed NSCLC were included in a prospective cohort study. All patients underwent single-phase contrast-enhanced SCT (using the fast tube voltage switching technique, 80–140 kV). SCT values (iodine content [IC], spectral slope pitch, and radiodensity increase) of malignant tissue (primary and metastases) and lymph nodes (LNs) were measured. Adrenal masses were evaluated in a virtual non-contrast series (VNS). If pulmonary embolism was present, pulmonary perfusion was analysed as an additional finding.

RESULTS: Fifty-two untreated primary NSCLC lesions were evaluable. Lung adenocarcinoma had significantly higher normalised IC (NIC: 19.37) than squamous cell carcinoma (NIC: 12.03; p=0.035). Pulmonary metastases were not significantly different from benign lung nodules. A total of 126 LNs were analysed and histologically proven metastatic LNs (2.08 mg/ml) had significantly lower IC than benign LNs (2.58 mg/ml; p=0.023). Among 34 adrenal masses, VNS identified adenomas with high sensitivity (91%) and specificity (100%). In two patients, a perfusion defect due to pulmonary embolism was detected in the iodine images.

CONCLUSION: SCT may contribute to the differentiation of histological NSCLC subtypes and improve the identification of LN metastases. VNS differentiates adrenal adenoma from metastasis. In case of pulmonary embolism, iodine imaging can visualise associated pulmonary perfusion defects.

* Guarantor and correspondent: F. Streitparth, Klinik und Poliklinik für Radiologie, LMU Klinikum der Universität München, Marchioninistr. 15, 81377 München, Germany. Tel.: +49 89 4400 73620.
E-mail address: Florian.Streitparth@med.uni-muenchen.de (F. Streitparth).
[1] U.F. and J.K. contributed equally to this study and share first authorship.

https://doi.org/10.1016/j.crad.2019.02.010
0009-9260/

Introduction

Lung cancer is the malignancy with the highest incidence worldwide and remains the leading cause of cancer-related death. Approximately 80% of lung cancers are classified as non-small cell lung cancer (NSCLC).[1,2] NSCLC has three major histological subtypes: squamous cell carcinoma (SCC), lung adenocarcinoma (LAC), and large cell neuroendocrine carcinoma. In conventional, single-energy computed tomography (CT) imaging, NSCLC lesions are described based on attenuation, morphology, and invasiveness. The response to treatment is monitored according to the Response Evaluation Criteria in Solid Tumours (RECIST 1.1).[3] Diagnosis of the exact subtype is often not possible based on tumour morphology alone.

Spectral CT (SCT) is a variant of dual-energy imaging that offers additional information on tumour properties through quantification of iodine concentration (IC), spectral slope analysis in monochromatic images, and the evaluation of a virtual non-contrast series (VNS). Dual-energy CT has been shown to allow specific characterisation of lung cancer tissue, for instance, in terms of histological grades or microvessel structure.[4,5] Quantitative material analysis in iodine images may contribute to a more precise subtype diagnosis and it had been shown that SCT can improve the differentiation of malignant and benign lesions.[6–8] Besides improving the evaluation of lung cancer primaries, dual-energy CT can also help in the detection of lymph node (LN) metastases[9,10] and in the differentiation of adrenal masses.[11,12] Adrenal metastases are common in lung cancer and are often difficult to distinguish from adenomas at single-energy contrast-enhanced CT. Additionally, SCT has also shown its value in quantifying pulmonary parenchymal perfusion.[13]

The present study was conducted to evaluate the SCT technique in the staging of NSCLC patients. Specifically, SCT values (IC, spectral slope pitch and radiodensity increase) were analysed regarding their potential to quantify tissue composition. The hypothesis of the study is that SCT values could help in further characterisation of NSCLC primaries and metastases. Conventional single energy CT relies on morphology rather than quantification of tumour components. SCT might help in the classification of primary tumours (regarding histological subtypes and grading) and in the differentiation of metastases and benign changes (pulmonary nodules, LNs, and adrenal masses). Quantification of SCT values has the potential to enable a more precise diagnosis and improve the diagnostic quality in staging of lung cancer.

Materials and methods

Patient characteristics and study design

From December 2016 until November 2017, 113 patients with confirmed NSCLC were included in this prospective cohort study. The study was approved by the ethics committee, and written informed consent was obtained from all study patients. Inclusion criteria for the study were (1) patients with histologically proven NSCLC based on either surgery or biopsy; (2) suspected lung cancer patients undergoing CT either as initial staging examination or for follow-up; (3) complete SCT protocol including contrast-enhanced spectral mode; and (4) patient age >18 years. Exclusion criteria were (1) contraindications to contrast-enhanced CT (impaired renal function, hyperthyroidism, iodine allergy); (2) inadequate CT examination; and (3) under-age patients.

CT technique

All patients underwent a single-phase SCT examination. SCT examinations were performed on a 64-row multisection CT system (third-generation dual-energy CT system, GE Revolution GSI, GE Healthcare, Chicago, Illinois, USA). SCT datasets were acquired using fast-tube voltage switching between 80 and 140 kVp. Patients were injected with 80 ml non-ionic contrast medium (Bayer Vital, Berlin, Germany, IC: 370 mg iodine/ml) via the antecubital vein at a rate of 4 ml/s. A single-phase SCT scan of the entire chest including the adrenals was acquired. A late-arterial-phase scan was acquired, starting 15 seconds after aortic enhancement (100 HU) using bolus tracking. Axial images with 0.625 mm thickness were generated using a standard soft-tissue kernel at a default energy of 70 keV.

Analysis of SCT parameters

The CT datasets were transferred to a workstation and analysed using dedicated SCT application software (GE Healthcare, GSI Volume Viewer). Post-processing was performed and iodine (water) images, monochromatic images (40–140 keV in 10 keV steps), and VNS were generated.

The following structures were measured and further analysed: (1) primary tumours: polygonal regions of interest (ROIs) including the entire tumour at its maximum cross-sectional diameter were placed. Tumour boundaries were identified in 70 keV images (representing conventional CT) in the tissue window setting (C: 40 W: 400). Adjacent atelectasis, mediastinal fat and major vessels were not included in the ROI. Additional ellipse-shaped ROIs (minimum diameter of 5 mm) were placed within the maximum diameter at the side of maximum enhancement for hot-spot analysis; (2) pulmonary nodules: maximum diameters were measured and ellipse-shaped ROIs were placed to include all metastatic tissue; (3) LNs: all LNs were measured in the N2 locations of the IASCL LN map.[14] Short and long axis diameters were measured; polygonal ROIs were placed in LN parenchyma. Fat in the hilar region was excluded when reasonably possible; (4) adrenal masses: polygonal ROIs including all tumour tissue were placed in adrenal masses; (5) in cases of pulmonary embolism: a circular ROI was placed in the affected lung tissue and contralateral/non-affected lung tissue (minimum diameter of 1 cm).

Additional circular ROIs were placed in the aorta, pulmonary trunk, non-malignant lung tissue, tracheal air, back muscles, and subcutaneous fat. All ROIs were manually placed by a radiologist with 5 years of experience in chest

imaging. Segmentation was performed in the SCT software application (GE Healthcare, GSI Volume Viewer). All ROIs were placed in the standard 70 keV images of the single-energy CT series (window setting C: 40 W: 400) and cloned to the post-processed SCT images.

Iodine (water) images: IC and normalised IC (NIC)

SCT enables tissue discrimination based on the attenuations at different energies emitted by the tube. The technique can be used to quantify specific materials as, e.g., iodine.[15] The IC of the ROIs was quantified in milligrams per millilitre using the GSI Volume Viewer. The NIC value was used to reduce variability caused by patient circulation attributes. NIC was calculated using the following formula: $IC_{lesion}/IC_{aorta} \times 100$.

When pulmonary embolism was present, parenchymal IC of the affected area was visually compared to surrounding unaffected lung parenchyma and quantified by ROI measurement.

Monochromatic images: spectral slope pitch (k)

Across the range of X-ray energies, different elements have different absorption fingerprints. A series of monochromatic images of various energy levels can be calculated by scanning at two different energy levels. This technique can analyse the composition of lesions, which characterises the spectral behaviour of different materials. The attenuation of certain lesions at different energy levels can then be presented as a virtual spectral curve.[16,17] Attenuation values were measured in ROIs placed in primary tumours and LNs at energy levels of 40, 50, 60, 70, 80, 90, 100, 110, 120, 130, and 140 keV and used to generate spectral attenuation slopes for each lesion measured. For statistical analysis, the pitch (k) of spectral slopes was calculated using the following formula: $(HU_{40\ keV} - HU_{120\ keV})/80$.

VNS: radiodensity increase

At single-energy CT, an increase in attenuation can be obtained by the attenuation difference of a lesion in a non-contrast series compared to a post-contrast series. Based on VNS, SCT can offer attenuation increase quantification in a single series. Attenuation values of all ROIs were obtained in VNS and in the corresponding contrast-enhanced series (70 keV). An increase in attenuation was calculated using the formula: $HU_{enhanced} - HU_{VNS}$.

Confirmation of diagnosis

All primary lung tumours were confirmed by histological examination of surgical or biopsy specimens. TNM stages, histological types, and grades were extracted from multidisciplinary tumour conference protocols. Pulmonary nodules were classified as metastases if confirmed by biopsy, or if new lesions occurred during the observation period (max. 12 months), or if unequivocal findings at combined 2-[^{18}F]-fluoro-2-deoxy-D-glucose (FDG)-positron-emission tomography (PET)/CT were present (high FDG uptake, morphology).[18] Non-metastatic pulmonary nodules were identified by negative biopsies or defined as pre-existing nodules with no size variation during the observation period.

LN involvement, node status, was based on histological specimens (surgery or biopsy) or if not available on FDG-PET/CT findings. FDG-PET/CT findings were only used to exclude mediastinal LN involvement in normal-sized nodes because of its high negative predictive value (NPV).[19,20]

Adrenal metastases were distinguished from adenomas by biopsy, or unequivocal imaging findings at magnetic resonance imaging (MRI; chemical shift imaging) or in FDG-PET/CT (tracer uptake and radiodensity evaluation).[21,22] New adrenal masses during the observation period (max. 12 months) were classified as metastases.

Statistical analysis

Statistical analysis was performed using SPSS version 21 (IBM, Armonk, NY, USA). Normal distribution of the data was excluded by the Kolmogorov–Smirnov test, and nonparametric tests were used. Bidirectional statistical analyses were performed using the non-parametric Mann–Whitney *U*-test and Spearman's correlation.

Results

Patient and lesion characteristics (Fig 1)

A total of 113 NSCLC patients were scanned using the above-described protocol. Adequate measurement was possible for 52 untreated primary NSCLC lesions. Small tumours (<5 mm maximum diameter) and tumours with poor margins (e.g., due to atelectasis) were excluded (n=22). Patients with prior treatment (n=39) were excluded from measurement of malignant tissue (primary lung tumour, LN metastases, and pulmonary metastases) and were only included for measurement of benign structures. In the group of 52 untreated primary lung cancers, there were 26 LAC, 14 SCC, and eight LCNEC. In four cases, definitive histology was not available (mixed type, equivocal histological findings). Histological grading was available for 22 cancers.

Thirty-one patients had pulmonary NSCLC metastases (22 with new lesions during observation; five with positive FDG-PET/CT findings, four biopsy proven). Twenty-eight patients had benign pulmonary nodules (22 with no dynamic during observation; six with non-malignant biopsy).

A total of 126 LNs were analysed regarding size criteria (<10 mm short axis: 68; ≥10 mm short axis: 58) in 74 patients. Histologically confirmed node status was available in 77 patients. Forty-five patients were histologically classified as N0/N1 (N–) and 32 as N2/N3 (N+). Fourteen patients without histologically confirmed node status had negative findings on FDG-PET/CT (normal-sized nodes and no significant FDG uptake) and were classified as N–. Out of these, 91 patients a total of 100 LNs were analysed.

Thirty-three patients had adrenal masses, among them 10 adrenal metastases (six with new lesions during observation; two with positive FDG-PET/CT findings, two with

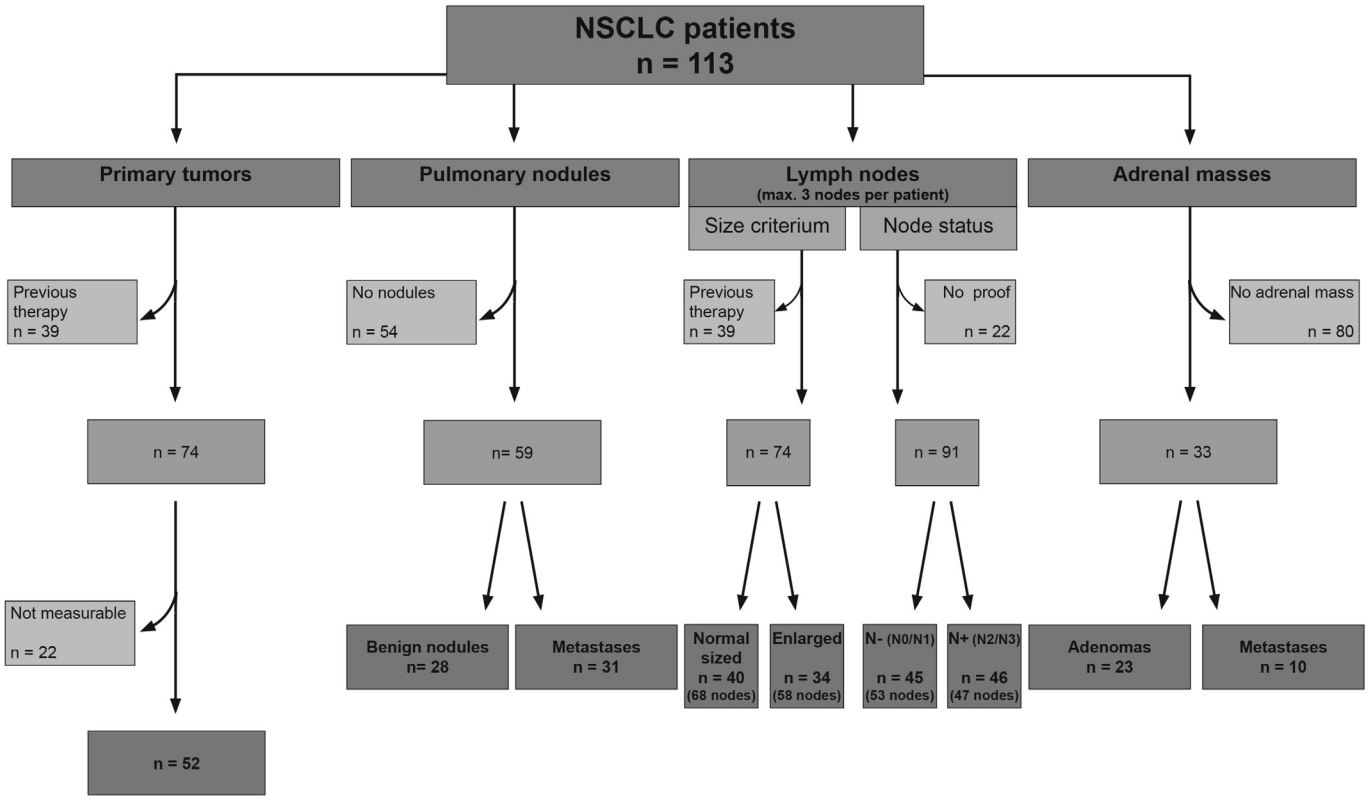

Figure 1 Patient and lesion characteristics.

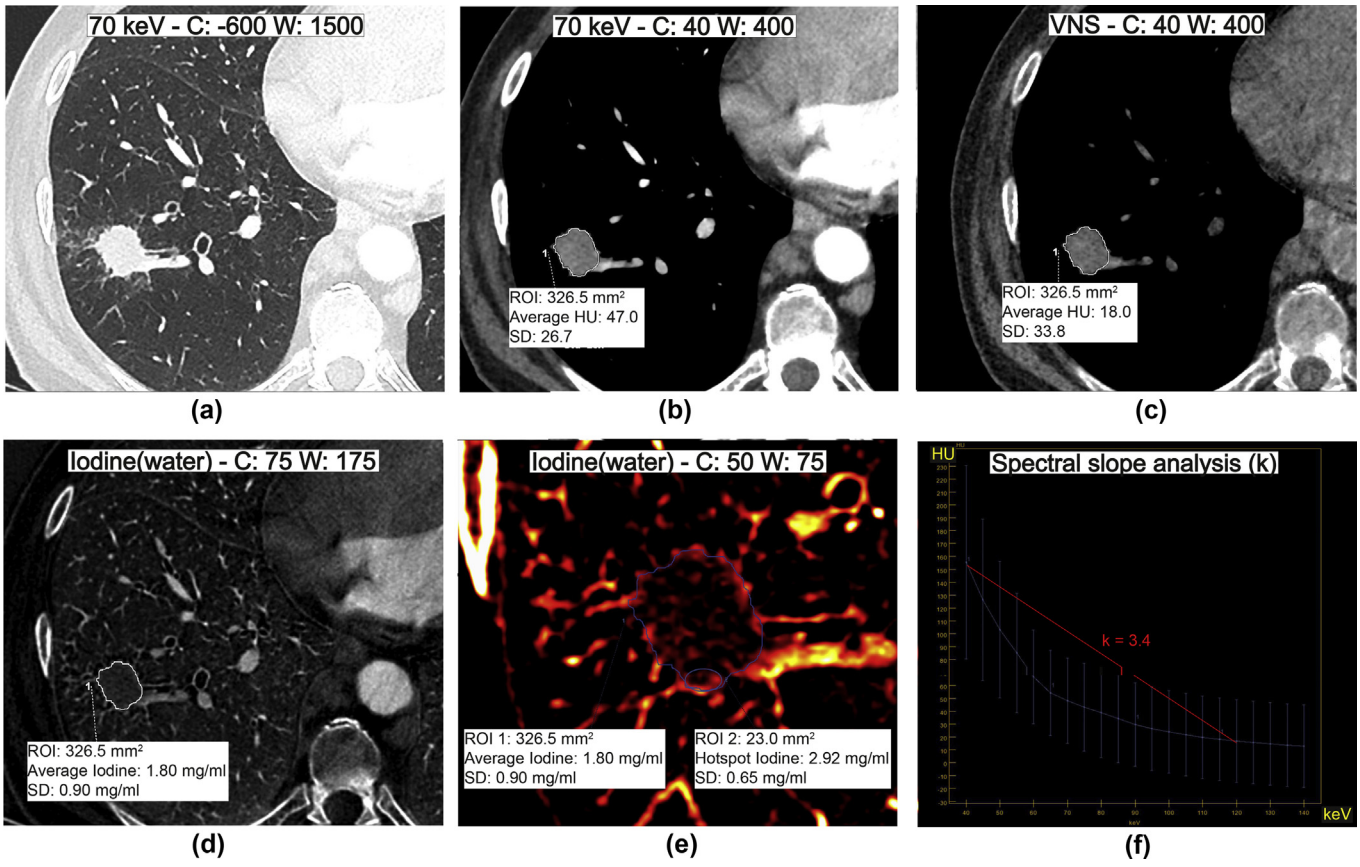

Figure 2 A 68-year-old patient with newly diagnosed LAC of the right lower lobe. (a) Imaging using 70 keV lung kernel; (b) 70 keV tissue kernel; (c) VNS; (d) iodine (water) images; (e) Iodine (water) images, hotspot analysis; (f) spectral slope analysis (40–140 keV).

positive biopsies) and 23 adenomas (nine with typical findings of adenoma in MRI; 12 with non-significant FDG uptake and typical findings for adenoma in unenhanced CT, two with negative biopsies). The additional finding of pulmonary embolism was observed in two patients.

Analysis of SCT parameters

Primary lung cancer (Fig 2)

Comparison of major histological types of lung cancer showed overall iodine values to be higher in LAC than in SCC. NIC was significantly higher in LAC (NIC: 19.37) than in SCC (NIC: 12.03; p=0.035; Fig 3). There were no significant differences between histological subtypes in spectral slope analysis and attenuation increase or hotspot analysis. Correlation analysis of SCT values with histological grades revealed slightly higher values for IC, NIC, attenuation increase, and spectral slope and lower values in the hotspot areas of high-grade lung cancers (G3 and G4); however, none of the differences were significant (Table 1).

Average IC (correlation coefficient: −0.577, p<0.001) and spectral slope values (correlation coefficient: −0.483, p<0.001) showed a significant negative correlation with tumour size.

Pulmonary nodules

There were no significant differences in SCT values between benign pulmonary nodules and lung metastases. IC (correlation coefficient: −0.595; p<0.001) and NIC (correlation coefficient: −0.600; p<0.001) significantly correlated with lesion size. Smaller lesions showed a higher IC than larger nodules (Table 2).

LNs (Fig 4)

LNs were divided into normal-sized (<10 mm short axis diameter) and enlarged (≥10 mm diameter) nodes. Normal-sized LNs (n=68) showed significantly higher IC (2.60 mg/ml), NIC (24.98), and higher k (2.50) than enlarged LNs (n=58; IC: 1.89 mg/ml; NIC: 18.39; k: 1.87; p<0.001 to 0.006). All measurements of LNs were obtained in the N2 localisation according to IASCL. They were divided according to their node status into N− (N0/N1) and N+ (N2/N3). LN metastases (N+; n=53; IC: 2.08 mg/ml) showed statistically significantly lower iodine values than non-metastatic LNs (N−; n=47; IC 2.58 mg/ml; p=0.023). NIC and increase in attenuation also showed a statistical trend towards lower values in metastases (N+; NIC: 19.63; attenuation increase: 36.13) than in benign nodes (N−; NIC: 25.45; attenuation increase: 45.85; p=0.074 and 0.076; Table 3, Fig 5).

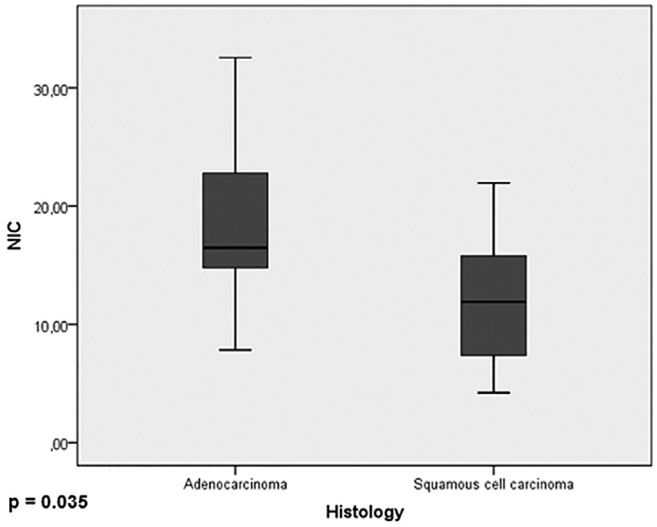

Figure 3 Boxplots showing NIC of LAC and SCC. LAC had significant higher NIC than SCC (p=0.035).

Table 1
Correlation of spectral computed tomography values with histological subtypes and histological grades of primary lung cancers.

Histology	LAC	SCC	p-Value
n	26	14	
IC (mg/ml)	2.01±1.05	1.29±0.69	0.237
NIC	19.37±8.11	12.03±6.04	0.035
Attenuation increase (HU)	30.10±16.81	23.19±7.60	0.447
Spectral slope	1.92±0.99	1.40±0.66	0.279
HS IC (mg/ml)	3.33±1.41	3.28±0.85	0.982
HS NIC	34.76±11.78	27.22±11.05	0.156
HS attenuation increase (HU)	55.19±32.56	55.10±23.42	0.597
Histological grade	Low grade (G1 & G2)	High grade (G3 & G4)	p-Value
n	9	13	
IC (mg/ml)	1.59±0.87	2.16±1.15	0.340
NIC	15.83±8.47	18.23±9.32	0.967
Attenuation increase (HU)	29.23±16.16	30.14±21.63	0.988
Spectral slope	1.53±0.82	2.06±1.08	0.340
HS IC (mg/ml)	3.53±1.20	3.36±1.41	0.967
HS NIC	35.34±15.61	28.75±12.53	0.299
HS attenuation increase (HU)	69.07±25.07	53.26±35.54	0.227

Values are mean±SD.
LAC, lung adenocarcinoma; SCC, squamous cell carcinoma; IC, iodine content; NIC, normalised iodine content; HU, Hounsfield unit; HS, hotspot.

Adrenal masses (Fig 6)

Evaluation of adrenal masses showed that VNS identified adrenal adenomas with 91% sensitivity and 100% specificity based on their typical imaging features (non-contrast attenuation <10 HU; Fig 6) Thirty-one of 33 lesions were correctly characterised by radiodensity evaluation in VNS. Only two adenomas did not fulfil the criteria of an

Table 2
Iodine values of benign and malignant pulmonary nodules.

	Metastases	Benign nodules	p-Value
n	31	28	
IC (mg/ml)	3.05±1.61	3.96±2.38	0.182
NIC	28.05±12.63	33.01±22.96	0.761
Spearman correlation	Correlation coefficient to diameter		
IC (mg/ml)	−0.595		<0.001
NIC	−0.600		<0.001

Values are mean±SD.
IC, iodine content; NIC, normalised iodine content.

Table 3
Correlation of spectral computed tomography values with lymph node size and metastatic status.

Size	<10 mm short axis	≥10 mm short axis	*p*-Value
n	68	58	
IC (mg/ml)	2.60±1.10	1.89±0.95	<0.001
NIC	24.98±16.80	18.39±9.68	0.006
Attenuation increase (HU)	42.08±26.96	35.24±22.03	0.195
Spectral slope	2.50±1.07	1.87±0.97	<0.001
Node status	N- (N0 and N1)	N+ (N2 and N3)	p-value
n	47	53	
IC (mg/ml)	2.58±1.13	2.08±1.05	0.023
NIC	25.45±18.30	19.63±10.67	0.074
Attenuation increase (HU)	45.85±27.14	36.13±22.93	0.076
Spectral slope	2.37±1.11	2.09±1.05	0.180

Values are mean±SD.
IC, iodine content; NIC, normalised iodine content; HU, Hounsfield unit.

attenuation value of <10 HU; however, these lesions showed high NIC (53.65 and 29.54) as well as relatively high IC (2.11 and 2.84 mg/ml). NIC was significantly higher in adenomas (NIC: 33.97) than in metastases (NIC: 19.95; p=0.022; Table 4).

Additional findings of pulmonary embolism (Fig 7)

In the two cases of pulmonary embolism, wedge-shaped perfusion defects of the affected lung parenchyma were visualised. The perfusion defects were not seen in the 70 keV series, which resembles single-energy CT. The perfusion defects could also be quantified by a significant decrease in IC in the affected areas (IC: 0.378 mg/ml) compared to the surrounding lung tissue (IC: 2.10 mg/ml).

The average radiation dose of the SCT scan was 340.18 (SD 88.53) mGy·cm (DLP) and 8.46 (SD 2.09) mGy (CTDI).

Discussion

The results of the present study showed significant differences in NIC of the major histological NSCLC subtypes. High-grade tumours showed higher IC as well as higher values of spectral slope pitch and attenuation increase than low-grade tumours; however, these findings were not statistically significant. In the present study, there were no significant differences between benign pulmonary nodules and pulmonary metastases. IC was significantly lower in metastatic LNs than in benign nodes. Adrenal metastases

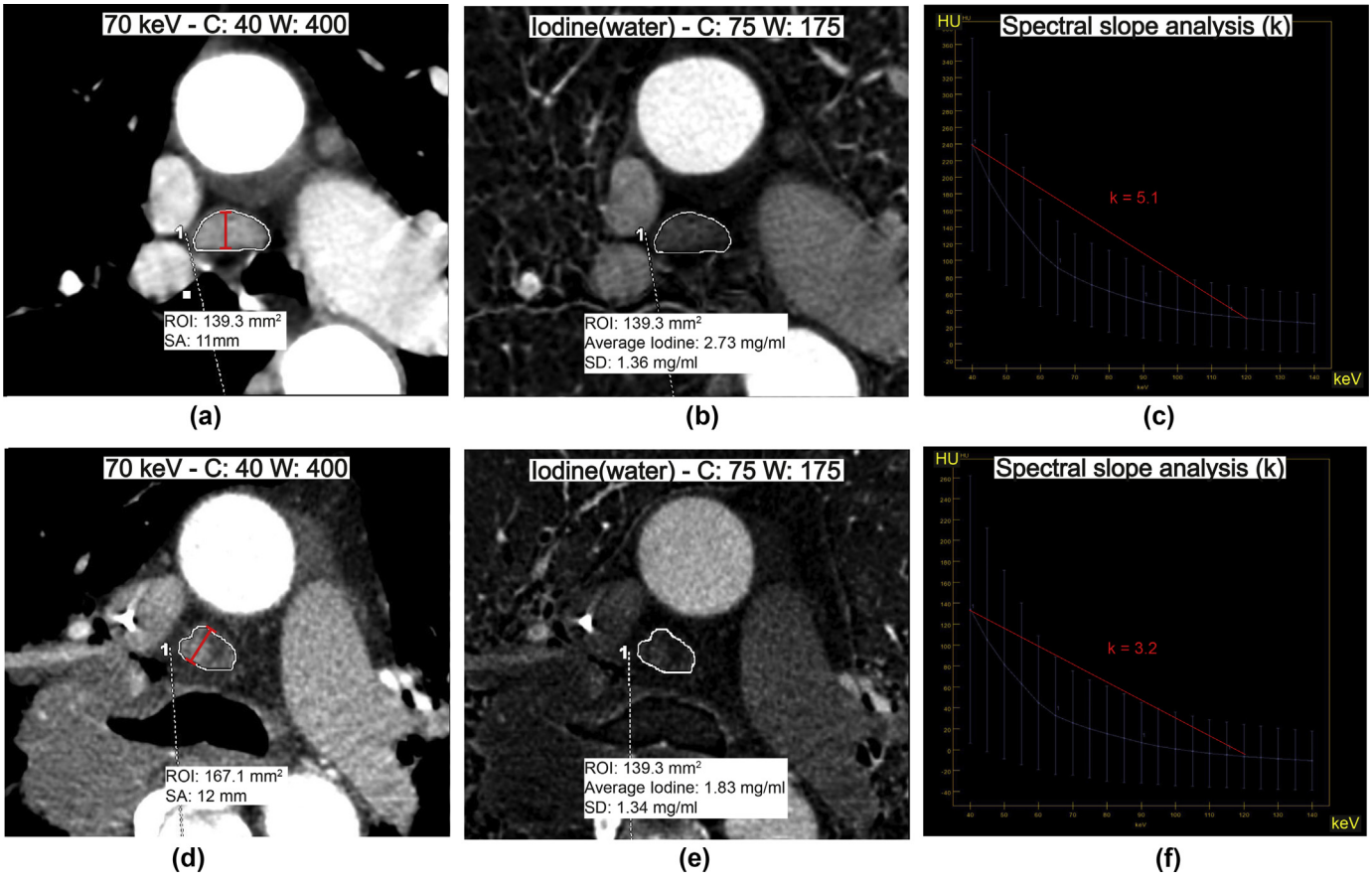

Figure 4 Upper row: a 76-year-old female patient with NSCLC without LN metastases. (a) Imaging using 70 keV lung kernel; (b) iodine (water) images; (c) spectral slope analysis. Bottom row: a 68-year-old male patient with mediastinal LN metastases. (d) Imaging using 70 keV lung kernel; (e) iodine (water) images; (f) spectral slope analysis. The LN metastasis had lower IC compared to benign LNs. Spectral slope analysis showed a steeper pitch in the benign LNs than in the metastatic LNs. Discrimination between metastasis and benign enlargement is not possible when only LN size is considered.

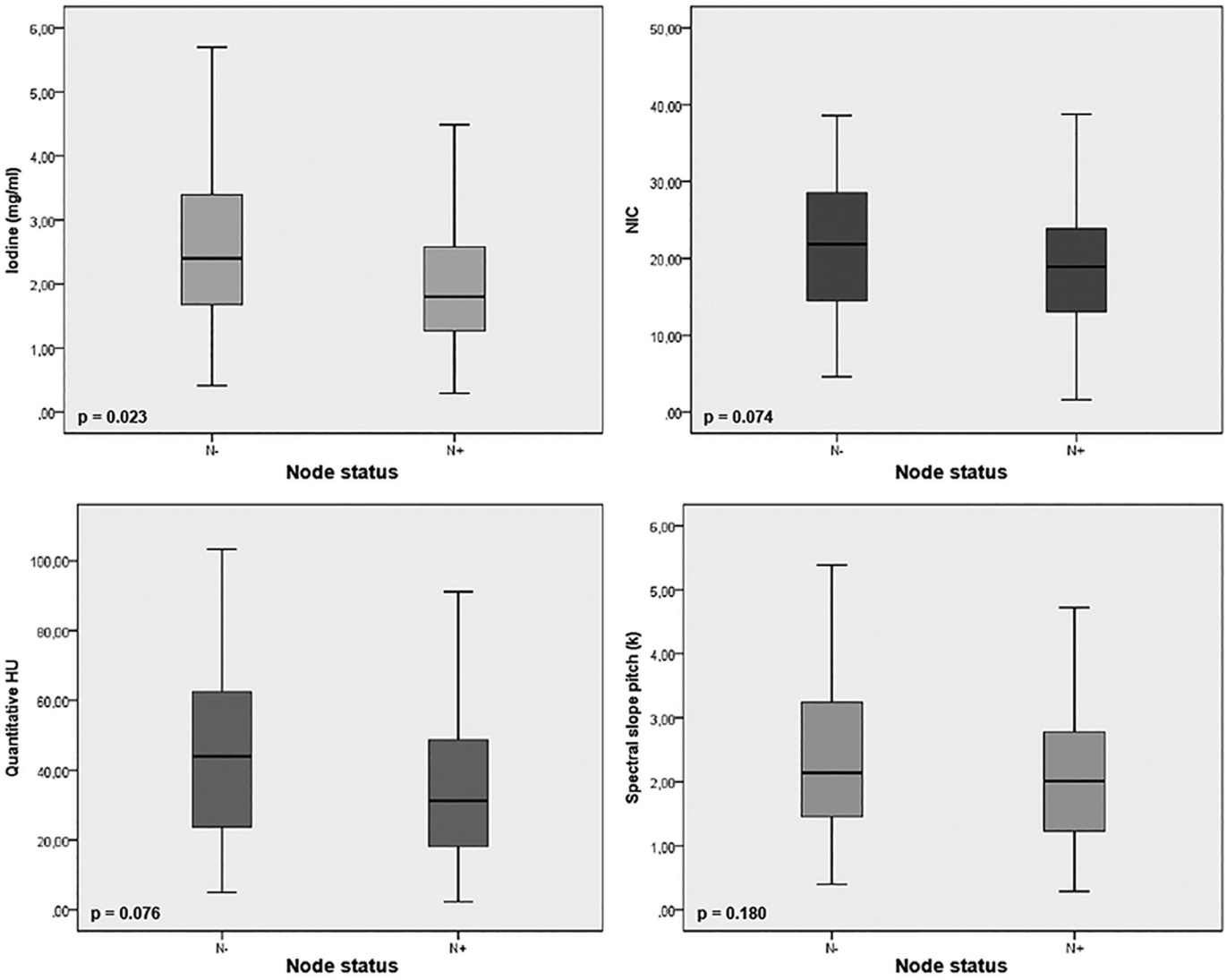

Figure 5 Boxplots comparing SCT values in non-metastatic (N−) and metastatic (N+) LNs. Metastatic LN had significantly lower IC than non-metastatic LN (p=0.023). A statistical trend was seen in NIC (p = 0.074) and attenuation increase (p = 0.076).

could be differentiated to adenomas by VNS with high sensitivity and specificity.

SCT provides advanced quantitative values (IC, spectral slope analysis, and attenuation increase) in a single-scan CT study. NSCLC and other lung neoplasms are routinely imaged using single-phase contrast-enhanced CT.[23] Characterisation of pulmonary malignancies therefore primarily depends on morphological criteria and strongly relies on follow-up studies if morphological criteria cannot help in distinguishing malignant from benign pulmonary lesions.[24] SCT with quantitative iodine analysis can help in the characterisation of vascularisation patterns[5]; however, IC strongly depends on the scan delay or the acquired contrast phase. The results of previous studies suggest that lung cancer enhancement peaks approximately 30–40 seconds after injection.[25,26] The use of bolus tracking is recommended for standardisation and better comparability. In the present study, a scan protocol with a fixed delay of 15 seconds after aortic enhancement was used to acquire late-arterial-phase images as was used by other investigators performing lung cancer perfusion studies.[26]

The overall average dose in the present study was lower than that of comparable contrast-enhanced, single-source, chest CT acquired with a standard tube voltage of 120 kV; however, the doses of SCT were higher than those of CT acquired with optimised chest protocols (iterative reconstruction, low tube voltage).[27–29] When a VNS is generated, the dose of a single-phase SCT is lower than that of a multiphase (unenhanced and contrast-enhanced) chest CT.[30] The dose applied in the present study is comparable to that previously published for dual-energy contrast-enhanced chest CT.[31]

In the present study, features of primary NSCLC were correlated with histology. Pulmonary adenocarcinoma had higher NIC than SCC; however, hotspot analysis revealed no significant differences between the histological subtypes.

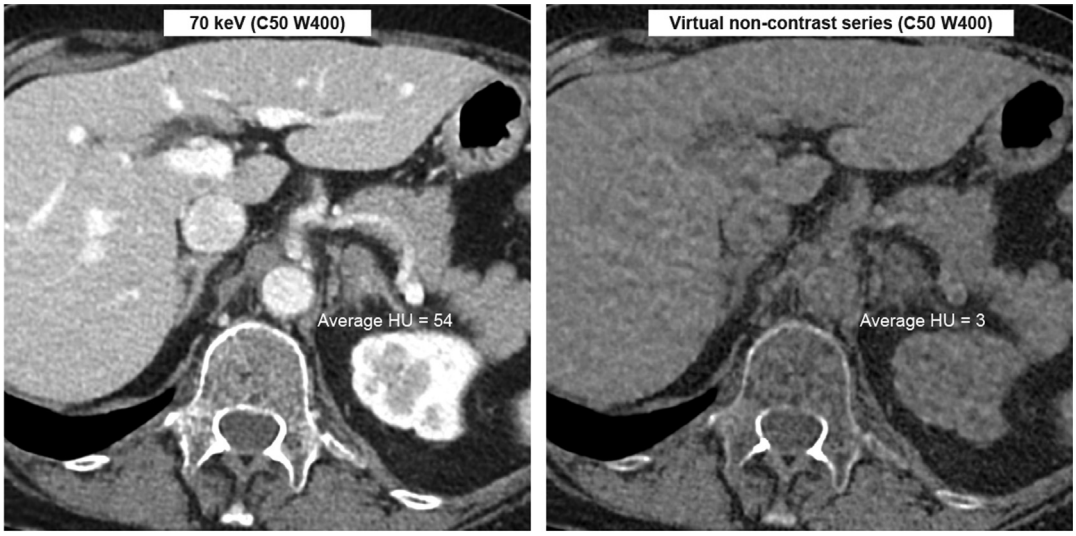

Figure 6 A 67-year-old female patient with NSCLC and a left adrenal mass. VNS shows low average attenuation of the mass and identifies this mass as a lipid-rich adenoma, which is not possible in contrast-enhanced single-source CT. (a) Imaging using 70 keV lung kernel, and (b) VNS.

Iodine hotspots were most frequently located in the tumour periphery. This pattern may be attributable to central necrosis, which lowers the overall average IC, but does not affect hotspots. It has been shown that necrosis is more common in SCC than in LAC[32] and that central necrosis is as an independent prognostic factor in NSCLC.[33] Improved visualisation by SCT could improve diagnostic accuracy, and IC might serve as a prognostic factor. Tumour necrosis has also been reported to be more common in more aggressive, high-grade tumours.[32] Contrary to previous reports,[34] SCT values did not significantly correlate with histological tumour grades in the present study. This finding might be attributable to the relatively small number of patients for whom histological grading was available in the present study and the fact that a uniform international grading system of NSCLC is still lacking.

Radiological LN assessment is an ongoing issue. The clinical determination of the N descriptor requires a multimodality approach in most cases (CT, PET/CT, oesophageal ultrasound, and/or endobronchial ultrasonography).[35] In CT, supplementing morphological assessment with perfusion analysis has been shown to be of value in the differentiation of metastatic and non-metastatic LNs by several investigators.[36–38] The most commonly used set of tumour response evaluation criteria (RECIST), however, only includes short axis LN diameter to discriminate metastatic from non-metastatic nodes.[3] The present results corroborate the usefulness of SCT in LN assessment. Iodine content, NIC, and spectral slope analysis contributed significantly to the detection of LN metastases. In patients with histological verification of LN status, metastatic LNs had lower iodine values and a lower spectral pitch than benign LNs. Enlarged LNs (according to RECIST criteria) also had significantly lower IC and lower pitch than normal-sized LNs. Consequently, SCT helped in distinguishing LN metastases in smaller LNs (<15 mm) not fulfilling the RECIST criteria.[3] The present results are in line with the findings of Yang *et al.*, who showed that especially spectral slope analysis of LNs improves specificity and sensitivity in identifying metastatic LNs compared with only considering short axis diameter.[9] This also applies to reactively enlarged LNs, which cannot be distinguished from metastatic nodes based on size alone. High iodine values have previously been reported for inflammatory LN enlargement.[10] Therefore, lower IC of enlarged LNs might allow a more reliable diagnosis of LN metastasis than measurement of short axis diameter alone.

Table 4
Spectral computed tomography values of adrenal adenomas and adrenal metastases.

	Adenoma	Metastases	*p*-Value
n	23	10	
Diameter (mm)	20.98±8.19	31.91±19.35	
IC (mg/ml)	2.46±0.95	1.80±0.92	0.133
NIC	33.97±19.39	19.95±17.31	0.022
Attenuation at CE (HU)	63.79±28.37	67.37±26.19	1.000
Attenuation at VNS (HU)	7.00±8.49	34.71±15.71	<0.001

Values are mean±SD.
IC, iodine content; NIC, normalised iodine content; HU, Hounsfield unit; CE, contrast enhanced; VNS, virtual non-contrast series.

In addition to quantitative material analysis, SCT offers the possibility of generating a VNS during post-processing.[39] This VNS can be used to quantify an increase in attenuation in a single-phase study and is especially useful in lung cancer patients, where it can add important information on adrenal masses. VNS showed typical characteristics of lipid-rich adenomas (average radiodensity values of <10 HU) in VNS, resulting in high sensitivity and specificity. These findings are consistent with previous studies showing VNS to be comparable to true unenhanced CT series in the evaluation of adrenal masses.[12] In the present study, only two adenomas (with attenuation values of >10 HU) could not be characterised by VNS, and these were lipid-poor adenomas; however, these lesions had relatively

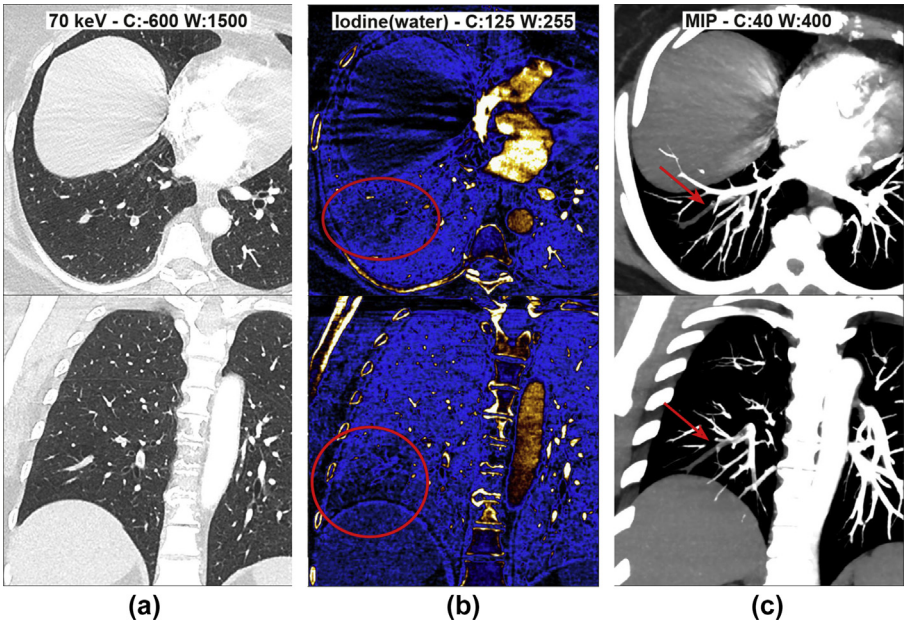

Figure 7 A 72-year-old male patient with NSCLC and incidentally detected pulmonary embolism of the right lower lobe (arrow) at follow-up CT. Iodine imaging shows a wedge-shaped perfusion defect in the right lower lobe (red circle). The perfusion defect cannot be seen in the 70 keV images: (a) 70 keV; (b) iodine (water) images; (c) maximum intensity projection (MIP) reconstruction.

high IC compared to metastases, suggesting that the combination of VNS attenuation and IC can help in even differentiating lipid-poor adenomas from adrenal metastases. SCT with its high sensitivity and specificity in the detection of lipid-rich adenomas can therefore dispense with an additional non-contrast CT series or even an MRI examination for comprehensive evaluation of adrenal masses; however, more patients need to be examined to corroborate these conclusions.

Another interesting feature of SCT is the visualisation and quantification of perfusion defects in pulmonary embolism.[40] In the present population, patients with pulmonary embolism showed typical wedge-shaped perfusion defects in the affected lung lobe with lower IC values than the surrounding non-affected lung tissue. This additional feature could help in determining the impact of vessel obstruction and offers additional information for the clinician.

The present study has some limitations. First, a relatively small number of patients was evaluated due to the strict inclusion criteria. Second, the results are applicable only to the CT systems from one vendor, as all examinations were performed on the same CT machine to allow comparability among patients. Third, definitive histopathological "proof" for all lesions (especially pulmonary and LN metastases) could not be provided. Another limitation is the inhomogeneity of the study population examined; however, the study population is representative of the lung cancer patients seen in a cancer centre during a 1-year study period and thus reflects everyday clinical life.

In conclusion, SCT and its quantitative values can help in the identification of histological NSCLC subtypes and could indicate grading. SCT values showed their usefulness in the detection of LN metastases and differentiation to benign LNs. With the aid of a VNS, SCT can differentiate between adrenal metastases and lipid-rich adenomas and, when used in conjunction with IC, can also help in the identification of lipid-poor adenomas. Visualisation and quantification of pulmonary perfusion defects in tumour-associated vessel obstruction or embolism offers additional information that is clinically relevant.

Funding

The authors state that this work has not received any funding.

Conflict of interest

The authors of this manuscript declare relationships with the following companies: Bernd Hamm is Grant Recipient for the Department of Radiology, Charité, and has further received funding from Abbott, AbbVie, Ablative Solutions, Accovion, Achaogen Inc., Actelion Pharmaceuticals, ADIR, Aesculap, AGO, AIF Arbeitsgemeinschaft industrieller Forschungsvereinigungen, AIO Arbeitsgemeinschaft Internistische Onkologie, Alexion Pharmaceuticals, Amgen, AO Foundation, Arena Pharmaceuticals, art photonics GmbH Berlin, ASR Advanced sleep research, Astellas, AstraZeneca, BARD, Bayer Healthcare, Bayer Schering Pharma, Bayer Vital, BBraun, Berlin-Brandenburger Centrum für Regenerative Therapien (BCRT), Berliner Krebsgesellschaft, Biotronik, Bioven, BMBF Bundesministerium für Bildung und Forschung, Boehring Ingelheimer, Boston Biomedical Inc., BRACCO Group, Brainsgate, Bristol-Myers Squibb, Cascadian Therapeutics, Inc., Celgene, CELLACT Pharma, Celldex Therapeutics, CeloNova BioSciences,

Charité research organisation GmbH, Chiltern, CCovance, CUBIST, Curis, Daiichi, DC Devices, Inc. USA, Delcath Systems, Dermira Inc., Deutsche Krebshilfe, Deutsche Rheuma Liga, DFG, DSM Nutritional Products AG, Dt. Stiftung für Herzforschung, Dynavax, Eisai Ltd., European Knowledge Centre, Mosquito Way, Hatfield, Eli Lilly and Company Ltd., EORTC, Epizyme, Inc., Essex Pharma, EU Programmes, Euroscreen S.A., Fibrex Medical Inc., Focused Ultrasound Surgery Foundation, Fraunhofer Gesellschaft, Galena Biopharma, Galmed Research and Development Ltd., Ganymed, GE, Genentech. Inc., GETNE (Grupo Español de Tumores Neuroendocrinos), Gilead Sciences, Inc., Glaxo Smith Kline, Glycotope GmbH, Berlin, Goethe Uni Frankfurt, Guerbet, Guidant Europe NV, Halozyme, Holaira Inc., ICON (CRO), Immunomedics Inc., Immunocore, Incyte, INC Research, Innate Pharma, InSightec Ltd., Inspiremd, inVentiv Health Clinical UK Ltd, Inventivhealth, IOMEDICO, IONIS, IPSEN Pharma, ISA Therapeutics, lsis Pharmaceuticals Inc., ITM Solution GmbH, Jansen, Kantar Health GmbH (CRO), Karyopharm Therapeutics, Inc., Kendle/MorphoSys AG, Kite Pharma, La Roche, Land Berlin, Lilly GmbH, Lion Biotechnology, Lombard Medical, Loxo Oncology, Inc, LSK BioPartners, USA; Lundbeck GmbH, LUX Biosciences, LYSARC, MacroGenics, MagForce, Medlmmune Inc., Medlmmune Limited, Medpace, Medpace Germany GmbH (CRO), MedPass (CRO), Medronic, Merck, Merrimack Pharmaceuticals Inc, MeVis Medical Solutions AG, Millennium Pharmaceuticals Inc., Mologen, MSD Sharp, NeoVacs SA, Nexus Oncology, Novartis, novocure, Nuvisan, Ockham oncology, Orion Corporation Orion Pharma, Parexel CRO Service, Perceptive, Pfizer GmbH, Pharma Mar, Pharmaceutical Research Associates GmbH (PRA), Pharmacyclics Inc., Philipps, PIQUR Therapeutics Ltd., Pluristem, Portola Pharmaceuticals, PPD (CRO), PRAint, Premier-research, Provectus Biopharmaceuticals, Inc., psi-cro, Pulmonx International Sárl, Quintiles Gmbh, Respicardia, Roche, Samsung, Sanofi, sanofis-aventis S.A, Schumacher GmbH, Seattle Genetics, Servier (CRO), SGS Life Science Services (CRO), Siemens, Silena Therapeutics, Spectranetics GmbH, Spectrum Pharmaceuticals, St. Jude Medical, Stiftung Wolfgang Schulze, Symphogen, Taiho Pharmaceutical Co., Taqu Therapeutics Ltd., Terumo Medical Corporation, Tesaro, TETEC AG, TEVA, Theorem, Theradex, Threshold Pharmaceuticals Inc., TNS Healthcare GmbH, Toshiba, UCB Pharma, Uni München, VDI/VDE, Winicker Norimed, Wyeth Pharma, Xcovery Holding Company, Zukunftsfond Berlin (TSB).

Acknowledgements

The study was in part presented at “European Congress of Radiology” 2017 and 2018 as well as at “Deutscher Röntgenkongress” 2018.

References

1. Ferlay J, Soerjomataram I, Dikshit R, *et al.* Cancer incidence and mortality worldwide: sources, methods and major patterns in GLOBOCAN 2012. *Int J Cancer* 2015;**136**(5):E359–86.
2. Travis WD, Brambilla E, Burke AP, *et al. WHO classification of tumours of the lung, pleura, thymus and heart*. 4th edition. Lyon: IARC Press; 2015.
3. Schwartz LH, Litiere S, de Vries E, *et al.* RECIST 1.1-Update and clarification: from the RECIST committee. *Eur J Cancer* 2016;**62**:132–7.
4. Lin LY, Zhang Y, Suo ST, *et al.* Correlation between dual-energy spectral CT imaging parameters and pathological grades of non-small cell lung cancer. *Clin Radiol* 2018;**73**(4):412.e411–7.
5. Wu F, Zhou H, Li F, *et al.* Spectral CT imaging of lung cancer: quantitative analysis of spectral parameters and their correlation with tumour characteristics. *Acad Radiol* 2018;**25**(11):1398–404.
6. Gonzalez-Perez V, Arana E, Barrios M, *et al.* Differentiation of benign and malignant lung lesions: dual-energy computed tomography findings. *Eur J Radiol* 2016;**85**(10):1765–72.
7. Chae EJ, Song JW, Seo JB, *et al.* Clinical utility of dual-energy CT in the evaluation of solitary pulmonary nodules: initial experience. *Radiology* 2008;**249**(2):671–81.
8. Wang G, Zhang C, Li M, *et al.* Preliminary application of high-definition computed tomographic gemstone spectral imaging in lung cancer. *J Comput Assist Tomogr* 2014;**38**(1):77–81.
9. Yang F, Dong J, Wang X, *et al.* Non-small cell lung cancer: spectral computed tomography quantitative parameters for preoperative diagnosis of metastatic lymph nodes. *Eur J Radiol* 2017;**89**:129–35.
10. Tawfik AM, Razek AA, Kerl JM, *et al.* Comparison of dual-energy CT-derived iodine content and iodine overlay of normal, inflammatory and metastatic squamous cell carcinoma cervical lymph nodes. *Eur Radiol* 2014;**24**(3):574–80.
11. Martin SS, Weidinger S, Czwikla R, *et al.* Iodine and fat quantification for differentiation of adrenal gland adenomas from metastases using third-generation dual-source dual-energy computed tomography. *Invest Radiol* 2018;**53**(3):173–8.
12. Ho LM, Marin D, Neville AM, *et al.* Characterization of adrenal nodules with dual-energy CT: can virtual unenhanced attenuation values replace true unenhanced attenuation values? *AJR Am J Roentgenol* 2012;**198**(4):840–5.
13. Okada M, Kunihiro Y, Nakashima Y, *et al.* Added value of lung perfused blood volume images using dual-energy CT for assessment of acute pulmonary embolism. *Eur J Radiol* 2015;**84**(1):172–7.
14. Rusch VW, Asamura H, Watanabe H, *et al.* The IASLC lung cancer staging project: a proposal for a new international lymph node map in the forthcoming seventh edition of the TNM classification for lung cancer. *J Thorac Oncol* 2009;**4**(5):568–77.
15. Gabbai M, Leichter I, Mahgerefteh S, *et al.* Spectral material characterization with dual-energy CT: comparison of commercial and investigative technologies in phantoms. *Acta Radiol* 2015;**56**(8):960–9.
16. Hurrell MA, Butler AP, Cook NJ, *et al.* Spectral Hounsfield units: a new radiological concept. *Eur Radiol* 2012;**22**(5):1008–13.
17. Wang Q, Shi G, Qi X, *et al.* Quantitative analysis of the dual-energy CT virtual spectral curve for focal liver lesions characterization. *Eur J Radiol* 2014;**83**(10):1759–64.
18. Bryant AS, Cerfolio RJ. The maximum standardized uptake values on integrated FDG-PET/CT is useful in differentiating benign from malignant pulmonary nodules. *Ann Thorac Surg* 2006;**82**(3):1016–20.
19. Postmus PE, Kerr KM, Oudkerk M, *et al.* Early and locally advanced non-small-cell lung cancer (NSCLC): ESMO Clinical Practice Guidelines for diagnosis, treatment and follow-up. *Ann Oncol* 2017;**28**(suppl_4):iv1–21.
20. Fischer BM, Mortensen J, Hansen H, *et al.* Multimodality approach to mediastinal staging in non-small cell lung cancer. Faults and benefits of PET-CT: a randomised trial. *Thorax* 2011;**66**(4):294–300.
21. Schwartz LH, Ginsberg MS, Burt ME, *et al.* MRI as an alternative to CT-guided biopsy of adrenal masses in patients with lung cancer. *Ann Thorac Surg* 1998;**65**(1):193–7.
22. Kumar R, Xiu Y, Yu JQ, *et al.* ^{18}F-FDG PET in evaluation of adrenal lesions in patients with lung cancer. *J Nucl Med* 2004;**45**(12):2058–62.
23. Novello S, Barlesi F, Califano R, *et al.* Metastatic non-small-cell lung cancer: ESMO Clinical Practice Guidelines for diagnosis, treatment and follow-up. *Ann Oncol* 2016;**27**(suppl 5):v1–27.
24. MacMahon H, Naidich DP, Goo JM, *et al.* Guidelines for management of incidental pulmonary nodules detected on CT images: from the Fleischner Society 2017. *Radiology* 2017;**284**(1):228–43.

25. Chen X, Xu Y, Duan J, *et al*. Correlation of iodine uptake and perfusion parameters between dual-energy CT imaging and first-pass dual-input perfusion CT in lung cancer. *Medicine (Baltimore)* 2017;**96**(28):e7479.
26. Fraioli F, Anzidei M, Serra G, *et al*. Whole-tumour CT-perfusion of unresectable lung cancer for the monitoring of anti-angiogenetic chemotherapy effects. *Br J Radiol* 2013;**86**(1029):20120174.
27. Kaul D, Grupp U, Kahn J, *et al*. Reducing radiation dose in the diagnosis of pulmonary embolism using adaptive statistical iterative reconstruction and lower tube potential in computed tomography. *Eur Radiol* 2014;**24**(11):2685–91.
28. Schafer ML, Ludemann L, Boning G, *et al*. Radiation dose reduction in CT with adaptive statistical iterative reconstruction (ASIR) for patients with bronchial carcinoma and intrapulmonary metastases. *Clin Radiol* 2016;**71**(5):442–9.
29. Kahn J, Kaul D, Grupp U, *et al*. Computed tomography in cystic fibrosis: combining low-dose techniques and iterative reconstruction. *J Comput Assist Tomogr* 2017;**41**(4):668–74.
30. Buty M, Xu Z, Wu A, *et al*. Quantitative image quality comparison of reduced- and standard-dose dual-energy multiphase chest, abdomen, and pelvis CT. *Tomography* 2017;**3**(2):114–22.
31. Renapurkar RD, Primak A, Azok J, *et al*. Attenuation-based kV pair selection in dual source dual energy computed tomography angiography of the chest: impact on radiation dose and image quality. *Eur Radiol* 2017;**27**(8):3283–9.
32. Al-Nafussi AIHD. *Histological diagnosis of tumours by pattern analysis*. London: Arnold; 1997.
33. Swinson DE, Jones JL, Richardson D, *et al*. Tumour necrosis is an independent prognostic marker in non-small cell lung cancer: correlation with biological variables. *Lung Cancer* 2002;**37**(3):235–40.
34. Iwano S, Ito R, Umakoshi H, *et al*. Evaluation of lung cancer by enhanced dual-energy CT: association between three-dimensional iodine concentration and tumour differentiation. *Br J Radiol* 2015;**88**(1055):20150224.
35. El-Sherief AH, Lau CT, Carter BW, *et al*. Staging lung cancer: regional lymph node classification. *Radiol Clin North Am* 2018;**56**(3):399–409.
36. Bisdas S, Baghi M, Smolarz A, *et al*. Quantitative measurements of perfusion and permeability of oropharyngeal and oral cavity cancer, recurrent disease, and associated lymph nodes using first-pass contrast-enhanced computed tomography studies. *Invest Radiol* 2007;**42**(3):172–9.
37. Liu Y, Bellomi M, Gatti G, *et al*. Accuracy of computed tomography perfusion in assessing metastatic involvement of enlarged axillary lymph nodes in patients with breast cancer. *Breast Cancer Res* 2007;**9**(4):R40.
38. Spira D, Wecker M, Spira SM, *et al*. Does volume perfusion computed tomography enable differentiation of metastatic and non-metastatic mediastinal lymph nodes in lung cancer patients? A feasibility study. *Cancer Imaging* 2013;**13**(3):323–31.
39. Ananthakrishnan L, Rajiah P, Ahn R, *et al*. Spectral detector CT-derived virtual non-contrast images: comparison of attenuation values with unenhanced CT. *Abdom Radiol (NY)* 2017;**42**(3):702–9.
40. Zhang LJ, Zhou CS, Schoepf UJ, *et al*. Dual-energy CT lung ventilation/perfusion imaging for diagnosing pulmonary embolism. *Eur Radiol* 2013;**23**(10):2666–75.